# Ghost Identification for QR Codes and Fingerprints with Thermal Light Modulation

Fei Lin, Ling Hong, Haoxu Guo, Xiaodong Qiu,[*] and Lixiang Chen[†]

*Department of Physics, Xiamen University, Xiamen 361005, China*

Ghost imaging with thermal light is a well-known imaging technique in which the light beam used for image reconstruction does not necessarily interact with the object. However, ghost imaging is generally time-consuming due to data acquisition and complex algorithm. Thus a fundamental question arises as to whether we can realize object identification without the need of reconstructing the full ghost images. Here we present a protocol of thermal-light-based object identification in a nonlocal manner, i.e., ghost identification, to answer this question positively. We employ a holography-type method to add an auxiliary planar phase together with the conjugate Fourier spectrum of the test object to the thermal light source, which revives the coherent transfer of complex spectrum from thermal light modulation to the second-order correlation function, regardless of no entanglement. In our experiment, we succeed in demonstrating the fairly good performance of ghost identification for both simple geometric objects and quick response codes, and particularly for fingerprints. Our protocol can find direct applications in secure biosensing and covert detection where very low light illumination levels are needed.

## I. INTRODUCTION

In contrast to direct image acquisition methods, ghost imaging is a technique that utilizes the correlation properties of two spatially separated beams [1–3]. In a ghost imaging modality, two beams of correlated photons are used: one beam illuminates the unknown object (test arm) and is collected by a pointlike detector without spatial resolution, while the other beam (reference arm) is recorded with a spatially resolved detector, e.g., a CCD camera. Neither of the detectors alone can reproduce an image of the object, but after correlating the two measurements, the object appears like a "ghost" in the reference arm in which the photons never interacted with the object. The ghost imaging experiment can be traced to the work by Pittman *et al.* with a biphoton entangled source, and therefore was initially claimed to be a pure quantum effect [4,5]. Soon after, it was realized that ghost imaging was also possible with only classical correlations [6–12]. On the one hand, a long-standing debate has been sparked as to whether entanglement is truly necessary for ghost imaging. On the other hand, a good deal of attention has been given to the potential applications with ghost imaging, such as lensless ghost imaging [13–15], single-pixel three-dimensional cameras [16], photolithography [17,18], and environmental sensing [19]. However, acquiring a high-quality ghost image is generally time-consuming and inefficient, as one

sampling contains only little information about the object. In order to enhance the imaging efficiency and quality, a variety of ghost imaging algorithms have been proposed, e.g., compressive sensing ghost imaging [20], differential ghost imaging [21], and that with Fourier transform [22] or data-driven deep learning [23,24].

However, these image processing problems are usually computationally demanding with electronic computers and still need thousand frames to acquire a clear image. In certain scenarios, such as medical cytometry [25], remote sensing [26], and traffic control [27], one demands to leverage the nonlocal property of ghost imaging and at the same time to rapidly identify an object. Recently, we constructed a quantum equivalence of the Vander Lugt filter for quantum pattern recognition [28]. However, two-photon quantum entanglement is an essential prerequisite for our previous scheme. As is well known, both quantum entanglement and thermal light sources can be used for ghost imaging. Thus, a question arises naturally as to whether we can realize pattern recognition or object identification with thermal light only, regardless of zero quantum entanglement. This consideration is of crucial importance, as thermal light sources are economically less costly, more flexible in generation and modulation, less sensitive to the external environment, and thus more viable for practical applications [29]. Besides, thermal light and quantum entanglement are two fundamentally different light sources. We find that, unlike quantum correlation, the spatial spectrum of a test object cannot be well transferred from thermal light modulation to the

———————
[*]qxd@xmu.edu.cn
[†]chenlx@xmu.edu.cn

second-order correlation function, as the phase information is unfortunately canceled out. To resolve the problem, we present a holography-type method, i.e., by adding an auxiliary planar phase onto the test spectrum's conjugate phase, which revives the complex spectrum of the test object in the second-order correlation function, and thus enabling the ghost identification of a target from several reference objects in a nonlocal manner. Our protocol can be seen as a combination of pattern recognition and ghost imaging, and thus is termed as ghost identification. Recently, there have been some similar descriptions, e.g., ghost cytometry [25], ghost tomography [30], ghost polarimetry [31,32], and ghost projection [33], to reflect the extended functions based on different variants of the ghost imaging setup. In our experiment, we succeed in demonstrating the fairly good performance of ghost identification for both simple geometric objects and quick response (QR) codes, and particularly for fingerprints.

## II. EXPERIMENTAL SCHEME AND THEORETICAL ANALYSIS

The experimental setup of thermal light modulation-based ghost identification is sketched in Fig. 1. We make pseudothermal light by using a 633-nm He-Ne laser beam to illuminate a spatial light modulator (SLM) that displays a sequence of phase screens with Kolmogorov statistic [34,35], see inset (a) of Fig. 1, which are generated by adding the phase of the modulated light field on the Kolmogorov phase screen and then converted to diffraction gratings (see also Fig. 2 for details). Then an optical 4f system consisting of two lenses (L1 and L2) and an iris is used to select the first-order diffraction, via which the

plane of the SLM is imaged onto that of a beam splitter (BS). Thus we obtain the pseudothermal light field, $E_S(\rho)$, with $\rho$ representing the transverse coordinates of the pseudothermal source in the plane of the BS. Here, the coherence length of the generating pseudothermal source is roughly 0.0244 mm [36,37], which is much smaller than the object size (approximately 5 mm) (see Appendix A for details). Therefore, we assume that a fairly good spatial incoherence is obtained, namely $\langle E_S(\rho_1) E_S^*(\rho_2) \rangle = \delta(\rho_1 - \rho_2)$, where the superscript $*$ denotes the complex conjugate. For ghost identification, additionally, we need to multiply each of the phase screens by a desired spatial amplitude, $E_{\text{Test}}(\rho)$, being related to the test object. Thus the pseudothermal source after spatial modulation can be written as $E(\rho) = E_S(\rho) E_{\text{Test}}(\rho)$. After a 50:50 nonpolarizing BS, the light in the test arm probes an object, then is collected and detected by a single-pixel detector only. Here, another 4f system of L3 and L4 (with focal lengths $f_3$ and $f_4$) is used to reimage the plane of the BS onto that of CCD1 (note that only the central pixel of CCD1 is used as a single-pixel detector). The reference objects, $R(u_1)$, are just placed in the Fourier plane of L3-L4, with $u_1$ denoting the coordinates in the reference object plane. Accordingly, we can derive the impulse response function in the test arm as

$$
\begin{aligned}
h_1(r_1, \rho_1) &= \int \exp\left(-i\frac{k}{f_3}u_1\rho_1\right) R(u_1) \exp\left(-i\frac{k}{f_4}u_1 r_1\right) du_1 \\
&= \tilde{R}\left(k\left(\frac{\rho_1}{f_3} + \frac{r_1}{f_4}\right)\right),
\end{aligned}
\tag{1}
$$

where $k = 2\pi/\lambda$, $r_1$ are the transverse coordinates in the plane of CCD1, and $\tilde{R}$ denotes the Fourier transformation of the reference object $R(u_1)$. While in the other arm, we
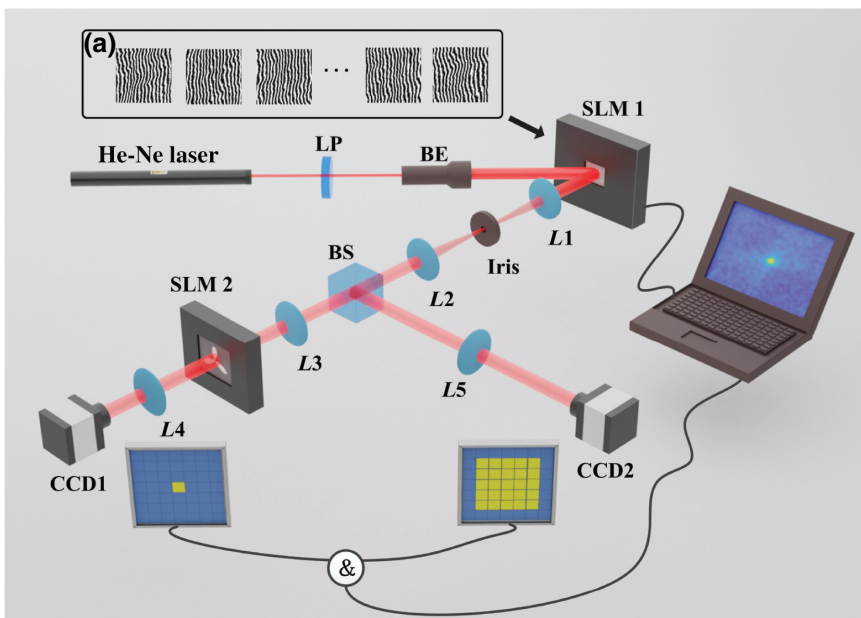


FIG. 1. Experimental setup of ghost identification with a holography-inspired spatial modulation of thermal light. See the text for details. Inset (a) shows the phase holograms displayed on SLM1.

let the light pass through a Fourier lens $L5$ (with a focal length of $f_5$), and place a spatially resolved CCD camera (CCD2) in its Fourier plane to record the intensity. Accordingly we have the impulse response function

$$h_2(r_2, \rho_2) = \exp\left(-i\frac{k}{f_5} r_2 \rho_2\right),\quad (2)$$

where $r_2$ denotes the transvers coordinates in the plane of CCD2. We can retrieve the "ghost correlation" by calculating the normalized second-order correlation function between the two CCD cameras, namely

$$g^{(2)}(r_1, r_2) = \frac{\langle I_1(r_1) I_2(r_2)\rangle}{\langle I_1(r_1)\rangle \langle I_2(r_2)\rangle}$$

$$= 1 + \frac{|\Gamma(r_1, r_2)|^2}{\langle I_1(r_1)\rangle \langle I_2(r_2)\rangle},\quad (3)$$

where $\langle\cdot\rangle$ denotes the ensemble average, $I_j(r_j) = E_j(r_j) E_j^*(r_j)$ is the optical intensity, and $\Gamma(r_1, r_2) = \langle E_1(r_1) E_2^*(r_2)\rangle$ is the first-order correlation function. Specifically, after substituting $E(r_1) = \int d\rho_1 h_1(r_1, \rho_1) E(\rho_1)$ and $E(r_2) = \int d\rho_2 h_2(r_2, \rho_2) E(\rho_2)$, we can obtain

$$\Gamma(r_1, r_2) = \int \tilde{R}\left[k\left(\frac{\rho_1}{f_3} + \frac{r_1}{f_4}\right)\right] |E_{\text{Test}}(\rho_1)|^2$$

$$\times \exp\left(i\frac{k}{f_5} r_2 \rho_1\right) d\rho_1.\quad (4)$$

It can be seen from Eq. (4) that if we modulate the thermal light to merely carry the test object's conjugate spectrum, $E_{\text{Test}}(\rho_1) = \tilde{T}^*([k/f_3]\rho_1)$, then the phase information of complex spectrum $\tilde{T}^*([k/f_3]\rho_1)$ will be totally canceled out as a result of $|E_{\text{Test}}(\rho_1)|^2$. Thus we cannot realize a successful ghost object identification. To resolve the problem, there are two subtle but important considerations. First, we consider only the conjugate phase of the Fourier spectrum, $\tilde{T}_N^*([k/f_3]\rho)$, rather than the full spectrum itself, to do the correlation, where $\tilde{T}_N([k/f_3]\rho) = \tilde{T}([k/f_3]\rho)/|\tilde{T}([k/f_3]\rho)|$. This is because phase-only filtering involves a narrower yet higher correlation peak compared with traditional matched filters [38]. Second, we consider a holography-type method for spatial modulation, i.e., to add an auxiliary planar phase $\exp(i2\pi\rho a)$ to the spectrum's pure phase. In this scenario, we can write the complex field of the pseudothermal source after spatial modulation as

$$E(\rho) = E_S(\rho)\left[\exp(i2\pi\rho a) + \tilde{T}_N^*\left(\frac{k}{f_3}\rho\right)\right],\quad (5)$$

where $a$ is an adjustable parameter. We illustrate in Fig. 2 the algorithm for preparing the holography-type thermal

light modulation of Eq. (5). We generate a variety of Kolmogorov phase screens through the approximated power spectral density of $\Phi = 0.023 r_0^{-5/3} f^{-11/3}$. By adding normally distributed deviations to the power spectral density, and taking the real part of the inverse Fourier transform, we can generate a single Kolmogorov phase screen, e.g., Fig. 2(a). Then a blazed grating of phase carrier, Fig. 2(b), is added to the phase screen, leading to the holographic grating with Kolmogorov statistics of Fig. 2(c) that can be used for pseudothermal light generation. In our holography-type modulation, we need to add the complex conjugate of the test object's Fourier spectrum of Fig. 2(d) together with an auxiliary planar phase of Fig. 2(e), then we extract the pure phase information of the sum field [see Fig. 2(f)]. By combining the pseudothermal light holograms of Fig. 2(c) and the spatial phase modulation of Fig. 2(f), we obtain the resultant pure-phase holographic grating of Fig. 2(g), which is displayed by SLM1 to implement the holography-type thermal light modulation.

In a standard ghost imaging modality, only the central pixel ($r_1 = 0$) of CCD1 is used as a single-pixel detector in the test arm. Thus we can rewrite Eq. (4) as

$$\Gamma(r_1 = 0, r_2) = \int d\rho_1 \exp\left(i\frac{kr_2}{f_5}\rho_1\right) \tilde{R}\left(\frac{k}{f_3}\rho_1\right)$$

$$\times \left[2 + \tilde{T}_N\left(\frac{k}{f_3}\rho_1\right) e^{i2\pi\rho_1 a}\right.$$

$$\left. + \tilde{T}_N^*\left(\frac{k}{f_3}\rho_1\right) e^{-i2\pi\rho_1 a}\right].\quad (6)$$

Mathematically, Eq. (6) can be equivalently rewritten as

$$\Gamma(r_1 = 0, r_2) = 2R(r_2)$$

$$+ T_N(r_2) * R(r_2) * \delta\left(r_2 + \frac{2\pi f_5}{k}a\right)$$

$$+ T_N(r_2) \star R(r_2) * \delta\left(r_2 - \frac{2\pi f_5}{k}a\right),\quad (7)$$

where $*$ and $\star$ denote the convolution and correlation operations, respectively, and the scale factor $m = -f_3/f_5$ for both test and reference objects has been omitted trivially. The correlation function of Eq. (7), behaving holographically, forms the key result of our present work: the first term reproduces the so-called ghost image of the reference object at zero-order diffraction, while the second term, centered at $r_2 = -(2\pi f_5/k)a$, is merely the convolution result of the test object and the reference one. Of particular interest is the third term, centered at $r_2 = (2\pi f_5/k)a$, which produces the cross-correlation signal, which therefore enables our protocol of object identification in a nonlocal manner, i.e., ghost identification.
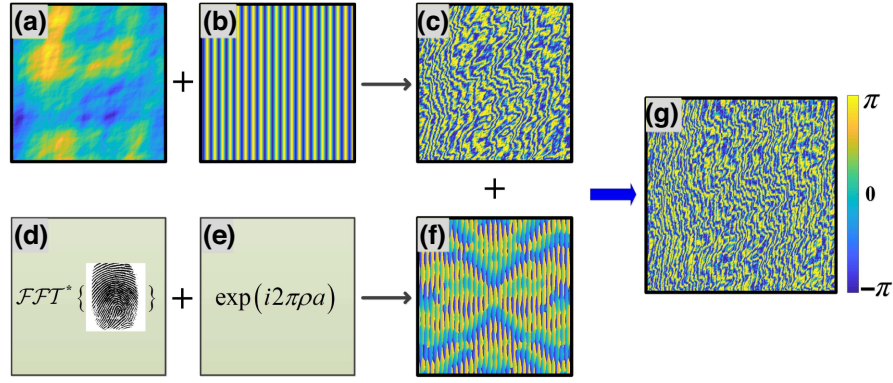
FIG. 2. The hologram algorithm for preparing pseudothermal light with holography-type modulation: (a) Kolmogorov phase screen, (b) blazed grating, (c) hologram with Kolmogorov statistics, (d) conjugate Fourier spectrum of the test object, (e) auxiliary planar phase, (f) holography-type spatial modulation, and (g) the final hologram.

## III. EFFICIENCY COMPARISON BETWEEN GHOST IDENTIFICATION AND GHOST IMAGING

In a standard ghost imaging modality, it is generally time-consuming to reconstruct the whole ghost image of an object, particularly under extremely low illumination levels. In contrast, ghost identification of an object is more efficient, as only a correlation peak signal is needed to be recorded. To show this technical advance, we take a simple clover object as a test example to demonstrate our protocol. In experiments, we preliminarily impart the conjugate phase of the clover's spectrum and a planar phase together onto the thermal light source, and at the same time we put the clover as the reference object (see Fig. 1). As indicated by Eq. (7), we are able to reconstruct the ghost image and the correlation signal simultaneously by measuring and calculating the second-order correlations, $g^{(2)}(r_1=0, r_2)$. We present our experimental observations in Fig. 3, which are obtained with sampling frame numbers from $N = 500$ to 4500, with an interval of 1000. In order to quantify the reconstruction quality for both ghost images and correlation signals, we use the contrast-to-noise ratio (CNR) [39], given by CNR = $(\langle G_{\text{in}} \rangle - \langle G_{\text{out}} \rangle)/\sqrt{\sigma_{\text{in}}^2 + \sigma_{\text{out}}^2}$, where $\langle G_{\text{in}} \rangle$ and $\langle G_{\text{out}} \rangle$ represent the ensemble average of the signal at any pixel inside and outside the desired regions, respectively, and $\sigma_{\text{in}}^2$ and $\sigma_{\text{out}}^2$ are the variances. We can see that both CNRs improve as the number of sampling frames increase. We can also see clearly that, for the same sampling number $N$, the CNR of the correlation signal is much better than that of the ghost image. Specifically, for $N = 200$, we can hardly recognize the clover image, as it is blurred in the noise background with a very low CNR = 0.70. In contrast, we can see a sharp correlation peak with CNR = 2.06, almost 3 times better than that of the ghost image. In order to get the same fairly good CNR = 2.06 for the

ghost image, one needs at least 4500 frames for the image reconstruction, as shown in Fig. 3. Thus, we conclude that ghost identification presents a faster yet more efficient method for object identification than the conventional ghost imaging.

## IV. RESULTS

To manifest the capacity of our protocol in identifying more complex patterns, we also take QR codes and fingerprints for ghost identification. A QR code is a type of matrix barcode that encrypts information into small black and white squares. It plays an important role in modern society due to its large information capacity, high reliability, and confidentiality [40,41]. In our experimental demonstration, we randomly generate five different QR codes as identification libraries. We present in Fig. 4 our experimental results of the cross-correlation matrix, $g^{(2)}(r_1=0, r_2)$. In each case, we take one specific QR code as the test object (see left axis), whose spectrum's conjugate phase together with a planar phase are imparted to the thermal light source, as mentioned above, in a holographylike manner. Then we take all five QR codes as the reference object (right axis), and ghost identification is done in sequence. Obviously, the correlation peaks only appear along the diagonal, as a result of pattern matching. For the off-diagonal, we cannot observe any evident matching signatures, as two different QR codes are compared. Unlike the biphoton entanglement case, there is a constant background of $g^{(2)}(r_1=0, r_2) = 1$ for thermal-light-based ghost identification, as is also indicated by Eq. (3). Then, we can calculate that the visibility of the cross-correlation matrix can reach approximately 25% for Fig. 4, and thus showing a fairly good performance of our protocol of ghost identification for QR codes.

As is well known, fingerprints are one of the most widely used biometric features to identify individuals
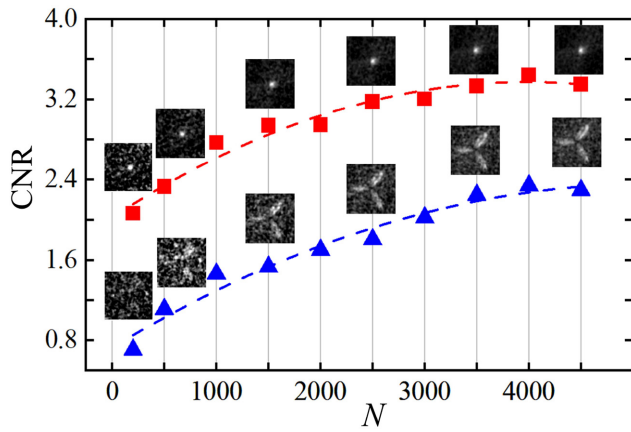
FIG. 3. CNR as a function of the measurement number $N$ for ghost image and cross-correlation signal. Each image is obtained by summing $N$ frames, with an exposure time of 10 ms for each frame. The dashed curves are guides to the eye.



FIG. 5. Experimental results of ghost identification for fingerprints. Each correlation signal is obtained by summing 2000 frames. The color-scale bar represents the value of $g^{(2)}$.

by virtue of their long-term invariance and uniqueness [42,43]. Here, we further demonstrate another experiment involving fingerprint identification, in which a sample fingerprint is compared with a set of known fingerprints stored in a database. In our experiment, we use five different fingerprints from the Fingerprint Verification Competition 2000 databases [44]. Then a $5 \times 5$ cross-correlation matrix is experimentally reconstructed in a similar way (see Fig. 5). Again, we observe that the cross-correlation peak signals are noticeable only along the diagonal for two identical fingerprints, but still disappear for the off-diagonal. It is noted that the maximal visibility for fingerprint identification is calculated to be approximately 12%, much lower than that for QR codes. After the normalization and thresholding operation, the recognition accuracies

are 91.61% and 89.37% for QR codes and fingerprints, respectively (see Appendix C for details).

## V. DISCUSSION

Theoretically, there are three main limiting factors for improving the performance of pattern recognition. The first one is the intensity of the zero-frequency component of an object's Fourier spectrum. For pattern recognition, the correlation signal comes from the object's high-frequency components, whereas the background noise arises from the zero-frequency component [45]. In other words, an object with a lower zero-frequency component can result in a higher correlation peak and signal-to-noise ratio. Generally, the zero-frequency component of a fingerprint is higher than that of a QR code (see Appendix B for details), and thus there is a higher correlation signal for a QR code, which is in agreement with the results in Figs. 4 and 5. Also, this is the reason why we need to accumulate more frames for fingerprint recognition. The second factor is that we must filter out the zero-frequency component in CCD1. Based on Klyshko's theory [4,8], we can equivalently consider the ghost identification setup with a back-projection picture. The point light source emitted from the central pixel ($r_1 = 0$) of CCD1, after being expanded and collimated by $L4$, goes back to illuminate the reference object. And then the light beam carrying the object information passes through $L3$ to conduct the Fourier transform. Here, by mixing the Fourier spectrum of the identity object into the thermal light, the BS can thus be seen as a matched filter [8,46]. Due to the light source emitted from the central pixel, the Fourier spectrum of the object can overlap with the matched filter perfectly. And thus after the Fourier transform of $L5$, there is a perfect correlation peak at CCD2. Based on the principle of the Fourier transform,
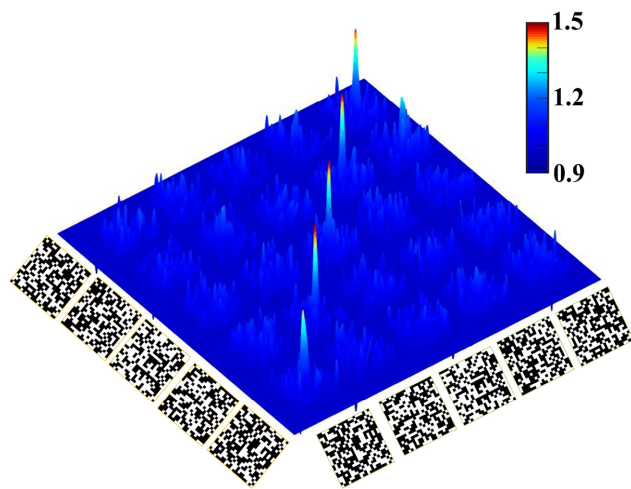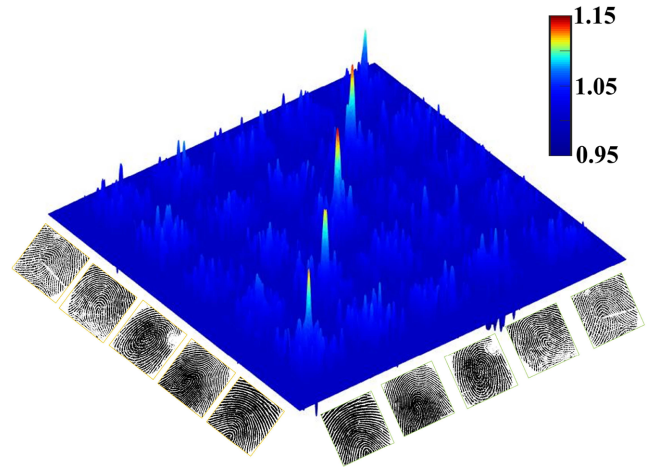


FIG. 4. Experimental results of ghost identification for QR codes. Each correlation signal is obtained by summing 500 frames. The color-scale bar represents the value of $g^{(2)}$.
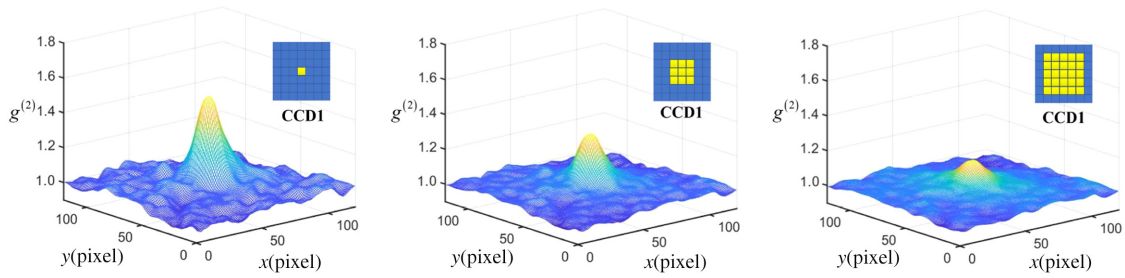
FIG. 6.   The correlation signal of clover under different collection areas in CCD1.

if the point light source is emitted from the other pixel ($r_1 \neq 0$), the light beam would illuminate the object with a tilt angle, and, accordingly, the Fourier spectrum of the object would mismatch with the matched filter located at the BS, thus generating a poor correlation signal. As for multipixels, the contribution among the mismatch correlation signals arising from $r_1 \neq 0$ pixels will bring more background and can decrease the recognition performance. For a quantitative illustration of this point, we analyze the experimental data, as presented in Fig. 6. From this we can see that the correlation signal decreases with increasing collected area in CCD1. The third limiting factor is the orthogonality of the test objects, which affects the recognition accuracy. As shown in Fig. 4, due to the slight similarity among different QR codes, there are also several weak correlation signals in the nondiagonal elements.

In experiments, the $4f$ imaging lens limits the operation spatial frequency band width of our system, i.e., the cutoff frequency. Taking the $x$ direction for example, the spatial frequency bandwidth $f_x$ is given by $0 < f_x < (ML_m/2f_3\lambda)$ [45,47], where $M$ denotes the magnification of the $4f$ system consisting of $L1$ and $L2$ and $L_m$ is the size of holographic grating loaded on SLM1 plane. In our present setup, $M = 0.5$, $L_m = 6$ mm (300 pixels), and $f_3 = 250$ mm, and thus the cut-off frequency is about 94 lines/cm. Accordingly, a suitable imaging lens is important for object identification. In addition, since the identity object is mixed into the thermal light, just filtering out the low-frequency part of the thermal light can lose some information and decrease the correlation signal. Finally, a better spatial overlap of the Fourier planes of the object with the modulated thermal light source at the BS is highly desirable, which could further improve the visibility.

## VI. CONCLUSION

In conclusion, we successfully implement a ghost identification protocol for a simple geometric object, QR codes, and fingerprints. In contrast to the biphoton entanglement case, here we only use a thermal light source, albeit with zero quantum entanglement. The key point to our scheme is the employment of a holography-type spatial light modulation, i.e., by imparting the conjugate phase of the test object's spectrum together with an auxiliary planar phase onto the thermal light source. Such an elaborated consideration avoids canceling out the phase information of the test object's spectrum in the second-order intensity correlation, and thus enabling object identification in a ghostly manner. Besides, our ghost identification is time-saving and efficient even at very low light illumination levels, in comparison with traditional ghost imaging that needs the full reconstruction of a two-dimensional image. We note that our protocol can be straightforwardly extended to the x-ray regime [48,49], and even to other massive particles such as atoms [37], electrons [50], etc. We also anticipate that our ghost identification can find direct applications in covert detection, secure biosensing, and environmental monitoring, where low-level illumination and noncontact operation are needed.
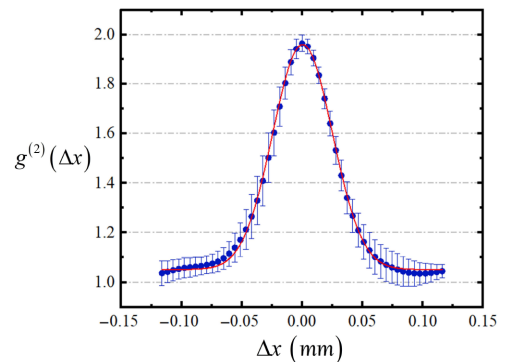
FIG. 7.   Normalized autocorrelation function $g^{(2)}(\Delta x)$ as a function of the coordinate $\Delta x$. The red line is a Gaussian fit of the correlation peak, which has a root-mean-square width of $\sigma = (0.0244 \pm 0.00028)$ mm, corresponding to the correlation length.
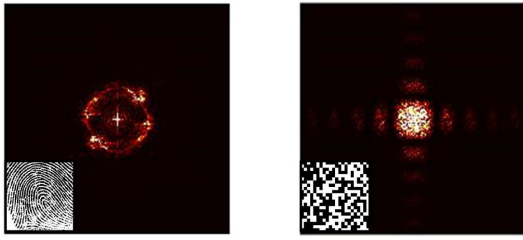
FIG. 8.    Fourier spectrum of fingerprint and QR code. Inset: the object's transmission image.

## APPENDIX A: COHERENCE LENGTH OF THERMAL LIGHT

We calculate the autocorrelation function $g^{(2)}(\Delta x)$ of the reference arm in CCD2, as illustrated in Fig. 7. Then we can acquire its coherence length $\sigma = (0.0244 \pm 0.000\,28)$ mm, which is much smaller than the object size (approximately 5 mm) [36,37]. Thus accordingly, the generated thermal source in our experiment can be seen as an incoherent source.

## APPENDIX B: FOURIER SPECTRUM ANALYSIS

Theoretically, the intensity of the zero-frequency component of an object's Fourier spectrum limits its recognition performance. Therefore, we analyze the Fourier spectrum of fingerprints and QR codes. As shown in Fig. 8, the zero-frequency component (dc component) of the fingerprint ($I_{dc}/I_{total} = 66.1\%$) is higher than that of the QR code ($I_{dc}/I_{total} = 48.8\%$ ), and thus there is a higher correlation signal for the QR code.



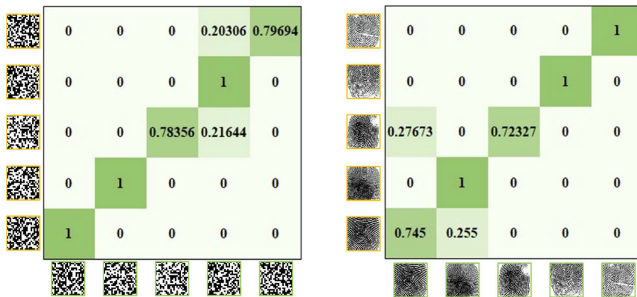FIG. 9.    The confusion matrix for QR codes (threshold approximately 1.1) and fingerprints (threshold approximately 1.04).

## APPENDIX C: ACCURACY EVALUATION

Here, we adopt the accuracy $\text{ACC} = \sum_i p_{ii}/\sum_{i,j} p_{ij}$ [51], to quantitatively evaluate the confidence level of the identification performance. $p_{ij}$ represents the normalized correlation signal. Due to the fact that the test objects are generally not orthogonal to each other, there are also correlation peaks in the nondiagonal elements (seen in Figs. 4 and 5). And the height of the correlation peak depends on the similarity between reference and test object. In order to remove the influence of nondiagonal elements, the general method is to conduct a thresholding operation [52,53], i.e., only recording the correlation signal above the threshold. After the normalization operation and thresholding operation, as shown in Fig. 9, accordingly, the recognition accuracies are 91.61% and 89.37% for QR codes and fingerprints, respectively.

[1] B. I. Erkmen and J. H. Shapiro, Ghost imaging: From quantum to classical to computational, Adv. Opt. Photonics **2**, 405 (2010).

[2] J. H. Shapiro and R. W. Boyd, The physics of ghost imaging, Quantum Inf. Process. **11**, 949 (2012).

[3] M. J. Padgett and R. W. Boyd, An introduction to ghost imaging: Quantum and classical, Philos. Trans. R. Soc. A **375**, 20160233 (2017).

[4] T. B. Pittman, Y. H. Shih, D. V. Strekalov, and A. V. Sergienko, Optical imaging by means of two-photon quantum entanglement, Phys. Rev. A **52**, R3429 (1995).

[5] A. F. Abouraddy, B. E. A. Saleh, A. V. Sergienko, and M. C. Teich, Role of Entanglement in Two-Photon Imaging, Phys. Rev. Lett. **87**, 123602 (2001).

[6] R. S. Bennink, S. J. Bentley, R. W. Boyd, and J. C. Howell, Quantum and Classical Coincidence Imaging, Phys. Rev. Lett. **92**, 033601 (2004).

[7] A. Gatti, E. Brambilla, M. Bache, and L. A. Lugiato, Correlated imaging, quantum and classical, Phys. Rev. A **70**, 013802 (2004).

[8] A. Valencia, G. Scarcelli, M. D'Angelo, and Y. Shih, Two-Photon Imaging with Thermal Light, Phys. Rev. Lett. **94**, 063601 (2005).

[9] F. Ferri, D. Magatti, A. Gatti, M. Bache, E. Brambilla, and L. A. Lugiato, High-Resolution Ghost Image and Ghost Diffraction Experiments with Thermal Light, Phys. Rev. Lett. **94**, 183602 (2005).

[10] J. Cheng and S. Han, Incoherent Coincidence Imaging and Its Applicability in X-ray Diffraction, Phys. Rev. Lett. **92**, 093903 (2004).

[11] R. S. Bennink, S. J. Bentley, and R. W. Boyd, "Two-Photon" Coincidence Imaging with a Classical Source, Phys. Rev. Lett. **89**, 113601 (2002).

[12] L. Chen, Quantum discord of thermal two-photon orbital angular momentum state: Mimicking teleportation to transmit an image, Light Sci. Appl. **10**, 148 (2021).

[13] M. Zhang, Q. Wei, X. Shen, Y. Liu, H. Liu, J. Cheng, and S. Han, Lensless Fourier-transform ghost imaging with

classical incoherent light, Phys. Rev. A **75**, 021803(R) (2007).

[14] X.-H. Chen, Q. Liu, K.-H. Luo, and L.-A. Wu, Lensless ghost imaging with true thermal light, Opt. Lett. **34**, 695 (2009).

[15] X.-F. Liu, X.-H. Chen, X.-R. Yao, W.-K. Yu, G.-J. Zhai, and L.-A. Wu, Lensless ghost imaging with sunlight, Opt. Lett. **39**, 2314 (2014).

[16] B. Sun, M. P. Edgar, R. Bowman, L. E. Vittert, S. Welsh, A. Bowman, and M. J. Padgett, 3D computational imaging with single-pixel detectors, Science **340**, 844 (2013).

[17] M. D'Angelo, M. V. Chekhova, and Y. Shih, Two-Photon Diffraction and Quantum Lithography, Phys. Rev. Lett. **87**, 013602 (2001).

[18] J. Xiong, D.-Z. Cao, F. Huang, H.-G. Li, X.-J. Sun, and K. Wang, Experimental Observation of Classical Subwavelength Interference with a Pseudothermal Light Source, Phys. Rev. Lett. **94**, 173601 (2005).

[19] N. D. Hardy and J. H. Shapiro, Computational ghost imaging versus imaging laser radar for three-dimensional imaging, Phys. Rev. A **87**, 023820 (2013).

[20] O. Katz, Y. Bromberg, and Y. Silberberg, Compressive ghost imaging, Appl. Phys. Lett. **95**, 131110 (2009).

[21] F. Ferri, D. Magatti, L. A. Lugiato, and A. Gatti, Differential Ghost Imaging, Phys. Rev. Lett. **104**, 253603 (2010).

[22] Z. Zhang, X. Ma, and J. Zhong, Single-pixel imaging by means of Fourier spectrum acquisition, Nat. Commun. **6**, 6225 (2015).

[23] M. Lyu, W. Wang, H. Wang, H. Wang, G. Li, N. Chen, and G. Situ, Deep-learning-based ghost imaging, Sci. Rep. **7**, 17865 (2017).

[24] F. Wang, C. Wang, C. Deng, S. Han, and G. Situ, Single-pixel imaging using physics enhanced deep learning, Photonics Res. **10**, 104 (2022).

[25] S. Ota, R. Horisaki, Y. Kawamura, M. Ugawa, I. Sato, K. Hashimoto, R. Kamesawa, K. Setoyama, S. Yamaguchi, K. Fujiu, K. Waki, and H. Noji, Ghost cytometry, Science **360**, 1246 (2018).

[26] X. Lu, X. Zheng, and Y. Yuan, Remote sensing scene classification by unsupervised representation learning, IEEE Trans. Geosci. Remote **55**, 5148 (2017).

[27] D. Cireşan, U. Meier, J. Masci, and J. Schmidhuber, Multicolumn deep neural network for traffic sign classification, Neural Netw. **32**, 333 (2012).

[28] X. Qiu, D. Zhang, W. Zhang, and L. Chen, Structured-Pump-Enabled Quantum Pattern Recognition, Phys. Rev. Lett. **122**, 123901 (2019).

[29] J.W. Goodman, eds., *Speckle Phenomena in Optics: Theory and Applications* (SPIE Press, Washington, 2020).

[30] A. M. Kingston, D. Pelliccia, A. Rack, M. P. Olbinado, Y. Cheng, G. R. Myers, and D. M. Paganin, Ghost tomography, Optica **5**, 1516 (2018).

[31] P. Janassek, S. Blumenstein, and W. Elsässer, Recovering a hidden polarization by ghost polarimetry, Opt. Lett. **43**, 883 (2018).

[32] S. Restuccia, G. M. Gibson, L. Cronin, and M. J. Padgett, Measuring optical activity with unpolarised light: Ghost polarimetry. ArXiv:2208.08199 (2022).

[33] David Ceddia and David M. Paganin, Ghost projection, Phys. Rev. A **105**, 013512 (2022).

[34] O. S. Magaña-Loaiza, M. Mirhosseini, R. M. Cross, S. M. H. Rafsanjani, and R. W. Boyd, Hanbury Brown and Twiss interferometry with twisted light, Sci. Adv. **2**, e1501143 (2016).

[35] Z. Yang, O. S. Magaña-Loaiza, M. Mirhosseini, Y. Zhou, B. Gao, L. Gao, S. M. H. Rafsanjani, G.-L. Long, and R. W. Boyd, Digital spiral object identification using random light, Light Sci. Appl. **6**, e17013 (2017).

[36] A. Gatti, M. Bache, D. Magatti, E. Brambilla, F. Ferri, and L. A. Lugiato, Coherent imaging with pseudo-thermal incoherent light, J. Mod. Opt. **53**, 739 (2006).

[37] R. I. Khakimov, B. M. Henson, D. K. Shin, S. S. Hodgman, R. G. Dall, K. G. H. Baldwin, and A. G. Truscott, Ghost imaging with atoms, Nature **540**, 100 (2016).

[38] J. L. Horner and P. D. Gianino, Phase-only matched filtering, Appl. Opt. **23**, 812 (1984).

[39] P. Zerom, Z. Shi, M. N. O'Sullivan, K. W. C. Chan, M. Krogstad, J. H. Shapiro, and R. W. Boyd, Thermal ghost imaging with averaged speckle patterns, Phys. Rev. A **86**, 063817 (2012).

[40] G. J. Garateguy, G. R. Arce, D. L. Lau, O. P. Villarreal, and Q. R. Images, Optimized image embedding in QR codes, IEEE Trans. Image Process. **23**, 2842 (2014).

[41] T. Yuan, Y. Wang, K. Xu, R. R. Martin, and S. M. Hu, Two-layer QR codes, IEEE Trans. Image Process. **28**, 4413 (2019).

[42] N. Kaushal and P. Kaushal, Human identification and fingerprints: A review, J. Biom. Biostat. **2**, 1000123 (2011).

[43] P. J. Phillips, A. Martin, C. L. Wilson, and M. Przybocki, An introduction evaluating biometric systems, Computer **33**, 56 (2000).

[44] D. Maio, D. Maltoni, R. Cappelli, J. L. Wayman, and A. K. Jain, FVC2000: Fingerprint verification competition, IEEE Trans. Pattern Anal. Mach. Intell. **24**, 402 (2002).

[45] J.W. Goodman, eds., *Introduction to Fourier Optics* (Roberts and Company Publishers, New York, 2005).

[46] G. Scarcelli, V. Berardi, and Y. Shih, Phase-conjugate mirror via two-photon thermal light imaging, Appl. Phys. Lett. **88**, 061106 (2006).

[47] W. Lukosz, Optical systems with resolving powers exceeding the classical limit. II, J. Opt. Soc. Am. **56**, 1463 (1966).

[48] H. Yu, R. Lu, S. Han, H. Xie, G. Du, T. Xiao, and D. Zhu, Fourier-Transform Ghost Imaging with Hard X Rays, Phys. Rev. Lett. **117**, 113901 (2016).

[49] D. Pelliccia, A. Rack, M. Scheel, V. Cantelli, and D. M. Paganin, Experimental X-Ray Ghost Imaging, Phys. Rev. Lett. **117**, 113902 (2016).

[50] S. Li, F. Cropp, K. Kabra, T. J. Lane, G. Wetzstein, P. Musumeci, and D. Ratner, Electron Ghost Imaging, Phys. Rev. Lett. **121**, 114801 (2018).

[51] Shuming Jiao, Jun Feng, Yang Gao, Ting Lei, Zhenwei Xie, and Xiaocong Yuan, Optical machine learning with incoherent light and a single-pixel detector, Opt. Lett. **44**, 5186 (2019).

[52] B. Javidi, Security information with optical techsnology, Phys. Today **50**, 27 (1997).

[53] Y. N. Hsu and H. H. Arsenault, Optical pattern recognition using circular harmonics expansion, Appl. Opt. **21**, 4016 (1982).